Research in Astronomy and Astrophysics, 26:025009 (7pp), 2026 February

https://doi.org/10.1088/1674-4527/ae2759
CSTR: 32081.14.RAA.ae2759

Quantifying the Relationship between Galaxy Specific Star Formation Rate and Halo Spin for Star-forming Galaxies

Wenxiao Xue[1,2], Zichen Hua[1,2], and Yu Rong[1,2]
[1] Department of Astronomy, University of Science and Technology of China, Hefei 230026, China; rongyua@ustc.edu.cn
[2] School of Astronomy and Space Sciences, University of Science and Technology of China, Hefei 230026, China
Received 2024 November 18; revised 2025 October 31; accepted 2025 November 26; published 2025 December 24

Abstract

Utilizing ALFALFA H I data, we investigate the relationship between specific star formation rate (sSFR) and halo spin across various star-forming galaxies. Our analysis reveals weak yet statistically significant positive correlation between sSFR and halo spin, irrespective of the galactic environment. This trend suggests that galaxies with higher spin parameters tend to host dynamically colder, gas-rich disks, sustaining elevated gas surface densities and prolonged star formation. These findings align with theoretical expectations of angular momentum-regulated gas accretion but highlight discrepancies with cosmological simulations, underscoring unresolved challenges in modeling baryonic feedback and star formation efficiency.

Key words: galaxies: statistics – galaxies: evolution – galaxies: formation

1. Introduction

In the standard galaxy formation model, halo spin is considered pivotal in galaxy formation and evolution, influencing morphology and regulating baryonic fraction (Mo et al. 1998; van den Bosch 1998; Diemand et al. 2005; Guo 2011; Amorisco & Loeb 2016; Desmond et al. 2017; Rong et al. 2017; Benavides et al. 2023). However, hydrodynamical simulations (e.g., Kim & Lee 2013; Di Cintio et al. 2019; Jiang 2019; Yang et al. 2023) have sparked debate on the role of halo spin in low-mass galaxies. For most dwarf galaxies, stellar distributions may be independent of or weakly dependent on halo spin, with concentrations and baryonic feedback exerting more significant influence on low-mass galaxy properties. Halos with shallower potential wells and lower concentrations exhibit stronger feedback effects, leading to reduced star formation efficiencies, lower stellar mass fractions, and more extended stellar distributions (Hopkins et al. 2012; Sawala et al. 2015; Kravtsov & Vikhlinin 2018; Sales et al. 2022; Liu et al. 2025; Rong et al. 2025). Despite extensive research, the influence of halo spin on galaxy structure and evolution remains incompletely understood and lacks consensus.

The star formation rate (SFR), a crucial parameter defining galaxy evolutionary state, is influenced by internal factors such as feedback, fuel supply, metallicity, and dust content (Springel 2000; Hayward et al. 2011; Hjorth et al. 2014; Grudić et al. 2018). Environmental factors also play a significant role in shaping the SFR (González & Padilla 2009; Tinker et al. 2017). Among the myriad of galaxy properties, the impact of halo properties on the SFR, while not direct, is paramount. Halos' mass and surface density (SD) have been shown to significantly affect SFRs in galaxies (Dahlem et al. 2006; Kimm 2009), yet the influence of halo spin on SFR remains uncertain. Rong et al. (2024b) propose a link between spin and SFR, suggesting that increased halo spin could hinder gas accretion and slow star formation processes. However, this proposed scenario requires further investigation.

H I surveys conducted with single-dish telescopes, such as the Arecibo Legacy Fast Alfa Survey (ALFALFA; Giovanelli 2005; Haynes 2018) and the undergoing FAST All Sky H I survey (Zhang et al. 2024), provide valuable H I spectra from numerous star-forming galaxies. These surveys offer crucial dynamical information on galaxies, facilitating the estimation of spin parameters for galaxies with varying SFRs and enabling the study of halo spin's impact on SFR.

In this study, we utilize a semi-analytic approach to estimate halo spin for each H I-bearing galaxy cataloged in ALFALFA and investigate the relationship between halo spins and stellar densities of galaxies. Section 2 introduces the sample data and outlines the methodology for estimating halo spin. Section 3 presents a statistical analysis of the dependence of galaxy stellar densities on halo spins. Our findings are summarized in Section 4.

2. Data

2.1. Sample and Specific Star Formation Rate

We draw our galaxy sample from ALFALFA, a comprehensive H I survey covering 6600 $\deg^2$ at high Galactic latitudes. The ALFALFA (α.100; Haynes 2018) catalog, released by Haynes (2018), includes ~31,500 sources with radial velocities below 18,000 $\mathrm{km\,s^{-1}}$. For each source, the

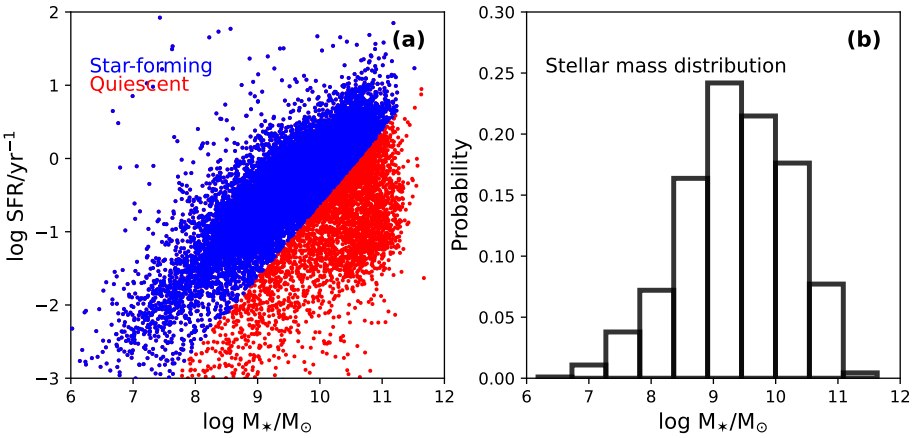

Figure 1. (a) SFR versus stellar mass for the star-forming (blue) and quiescent (red) galaxies. (b) Stellar mass distribution for the star-forming galaxies in this study.

catalog provides the H I spectrum signal-to-noise ratio (SNR), cosmological distance, 50% peak width of the H I line (W_{50}) corrected for instrumental effects, H I mass ($M_{\rm H\ I}$), among other properties.

We match ALFALFA galaxies with MPA-JHU DR7 SDSS measurements to obtain SFRs (Brinchmann et al. 2004) and stellar mass ($M_\star$) based on photometric fits. The specific SFR (sSFR) for each galaxy is then calculated as sSFR = SFR/$M_\star$ (yr^{-1}). To focus on star-forming galaxies, we select those with log sSFR $>\log(1/3t_{\rm H(z=0)}) \approx -10.62$ (Jing et al. 2021), where $t_{\rm H(z=0)}$ represents the Hubble time at redshift 0. After applying these selection criteria, our sample comprises 15,787 star-forming galaxies, consisting of 8187 low-mass ($M_\star < 10^{9.5}\,M_\odot$) systems and 7600 high-mass ($M_\star > 10^{9.5}\,M_\odot$) counterparts. As illustrated in panel (a) of Figure 1, the vast majority of these galaxies lie on the star-forming main sequence (Noeske et al. 2007; Schreiber et al. 2016), confirming their actively star-forming nature. Panel (b) of Figure 1 presents the stellar mass distribution of the selected sample.

2.2. Rotation Velocity and Halo Spin

The rotation velocity is given by $V_{\rm rot} = W_{50}/2/\sin\phi$, with inclination ϕ of the H I disk estimated via the optical axis ratio b/a (from Durbala et al. 2020) and $\sin\phi = \sqrt{(1-(b/a)^2)/(1-q_0^2)}$, setting $\phi = 90°$ for $b/a \leqslant q_0$. We assume $q_0 \sim 0.2$ for massive galaxies and $q_0 \sim 0.4$ (Rong et al. 2024a) for low-mass galaxies ($M_\star < 10^{9.5}M_\odot$). We exclude galaxies with $\phi < 50°$ or low SNR (< 10) to ensure accurate $V_{\rm rot}$ measurements.

Some H I-bearing galaxies exhibit velocity dispersion-dominated kinematics. These galaxies, identified by their H I line profiles exhibiting a "single-horned" shape (El-Badry 2018), pose challenges in accurately estimating rotation velocities and, consequently, halo spins. Following Hua et al. (2025a), we employ the kurtosis parameter $k_4 < -1.0$ to restrict our analysis to robust subsets of galaxies with double-horned H I profiles to exclude potential contamination from dispersion-dominated systems. After applying all selection criteria, our final sample comprises 2957 star-forming galaxies.

Assuming an isothermal halo model with negligible baryonic gravitational influence, the halo spin parameter $\lambda_{\rm h}$ is estimated as (Hernandez et al. 2007):

$$\lambda_{\rm h} \simeq 21.8\frac{R_{\rm H\,I,d}/{\rm kpc}}{(V_{\rm rot}/{\rm km\ s^{-1}})^{3/2}}, \quad (1)$$

where $R_{\rm H\ I,d}$ is the H I disk scale length, derived from:

$$\Sigma_{\rm H\,I}(R) = \Sigma_{\rm H\,I,0}\exp(-R/R_{\rm H\,I,d}), \quad (2)$$

where $\Sigma_{\rm H\ I,0}$ is the central SD of the H I disk. The total H I mass $M_{\rm H\ I}$ is linked to the scale length as

$$M_{\rm H\,I} = 2\pi\Sigma_{\rm H\,I,0}R^2_{\rm H\,I,d}. \quad (3)$$

Additionally, we introduce the H I radius $r_{\rm H\ I}$, defined as the radius at which the H I SD reaches $1\,M_\odot\,{\rm pc}^{-2}$. $r_{\rm H\ I}$ is calculated using the observed $r_{\rm H\ I}$–$M_{\rm H\ I}$ relation (Wang et al. 2016; Gault 2021): $\log r_{\rm H\,I} = 0.51\log M_{\rm H\,I} - 3.59$ (Wang et al. 2016; Gault 2021). Therefore, at $r_{\rm H\ I}$, we have

$$\Sigma_{\rm H\,I,0}\exp(-r_{\rm H\,I}/R_{\rm H\,I,d}) = 1\ M_\odot\ {\rm pc}^{-2}. \quad (4)$$

By using Equations (3) and (4), we can compute the value of $R_{\rm H\ I,d}$ for each galaxy in our sample, thereby enabling the estimation of the halo spin.

3. Results

Panels (a) and (b) of Figure 2 illustrate the sSFR–halo spin relation for low-mass ($M_\star < 10^{9.5}M_\odot$) and high-mass ($M_\star > 10^{9.5}M_\odot$) galaxies. Correlation analysis demonstrates a statistically significant, albeit weak, dependence of sSFR on halo spin, with correlation coefficients of CC $\approx$ 0.2 and CC $\approx$ 0.1 for the low-mass and high-mass regimes, respectively. The robustness of this trend is underscored by low p-values ($p = 2\times10^{-19}$ and $p = 1\times10^{-3}$ for the low-

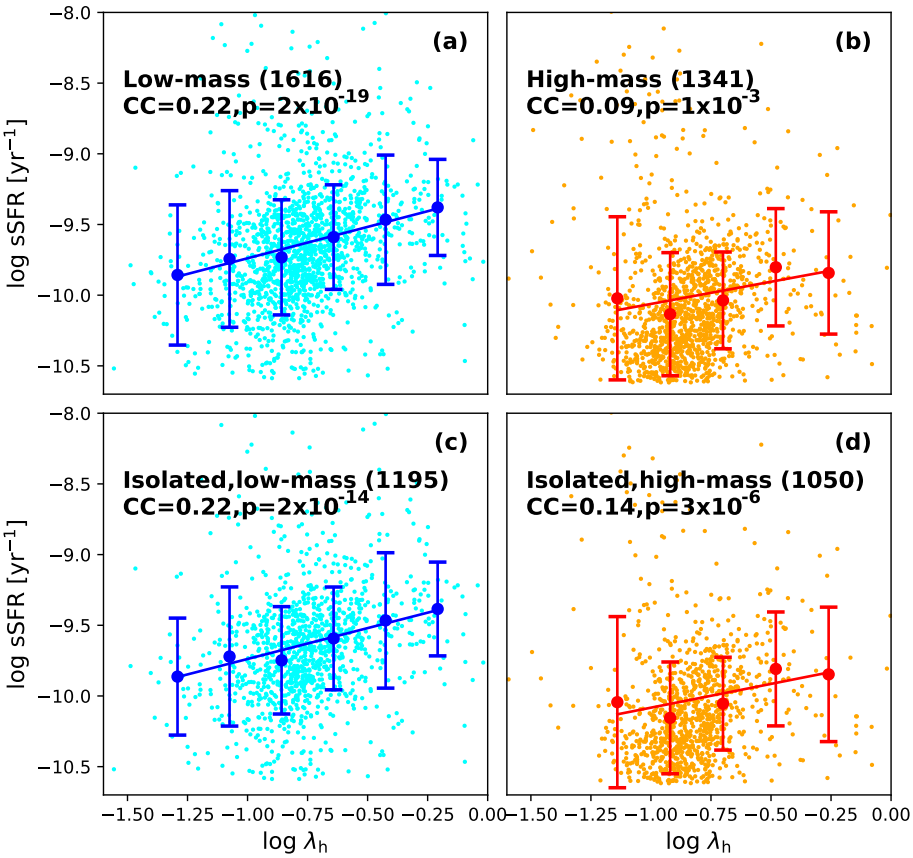

Figure 2. sSFR versus halo spin parameter for low-mass (left) and high-mass (right) galaxies. The top panels show the full star-forming galaxy sample, while the bottom panels focus on isolated galaxies. The numbers of galaxies are shown in the brackets of the corresponding panels. Median sSFR values with 1σ error bars for each bin in $\log \lambda_h$ are represented. Best-fit linear trends are indicated by the corresponding lines. CC and p-value for the subsamples are also shown in the corresponding panels.

and high-mass subsamples, respectively), confirming that the correlation, while modest in strength, is highly significant in both regimes. Notably, the relationship seems to be more pronounced in low-mass systems, plausibly suggesting a stronger coupling between halo spin and star formation efficiency in dwarf galaxies compared to their more massive counterparts.

Since environment also affects galaxy properties (e.g., Moore et al. 1996; Mayer et al. 2001; Mastropietro et al. 2005; Kazantzidis et al. 2011; Smith et al. 2015; Hua et al. 2025b), we control for environmental influences by using the galaxy group catalog by Saulder et al. (2016), applying a friends-of-friends algorithm to SDSS DR12 (Alam 2015) and 2MASS Redshift Survey data (Huchra 2012), adjusted for biases (e.g., Malmquist bias). The analysis of 2245 isolated galaxies-defined as systems located beyond three virial radii from any galaxy group-reveals a consistent, albeit weak, correlation between sSFR and halo spin (Figure 2, panels (c) and (d)). Statistically significant trends are observed for both low-mass (CC $= 0.22$, $p = 2 \times 10^{-14}$) and high-mass (CC $= 0.14$, $p = 3 \times 10^{-6}$).

4. Discussion and Conclusion

Using ALFALFA H I data, we examine sSFR–halo spin relationships for a range of star-forming galaxies. Our analysis reveals a weak but statistically significant correlation between them, independent of environment. Notably, star-forming main sequence galaxies exhibit increasing sSFR with higher spin parameters, with this trend being more pronounced in low-mass systems compared to their high-mass counterparts.

To ensure the robustness of this finding, we conducted multiple validation tests. First, we examine the sSFR–spin correlation across multiple inclination thresholds (30°, 40°, 60°, and 70°). As shown in Figure 3, the statistically significant correlation persists at all tested inclination angles, despite showing relatively weak correlation coefficients ($0.1 <$ CC < 0.3). This demonstrates that our results are robust against potential inclination-related biases in the H I kinematic measurements. Second, to verify the methodology dependence, we also recompute the spin parameter using stellar disk scale lengths ($R_{\star,d}$) instead of H I scale lengths ($R_{\mathrm{H\,I,d}}$) with Equation (1). The stellar scale lengths are derived

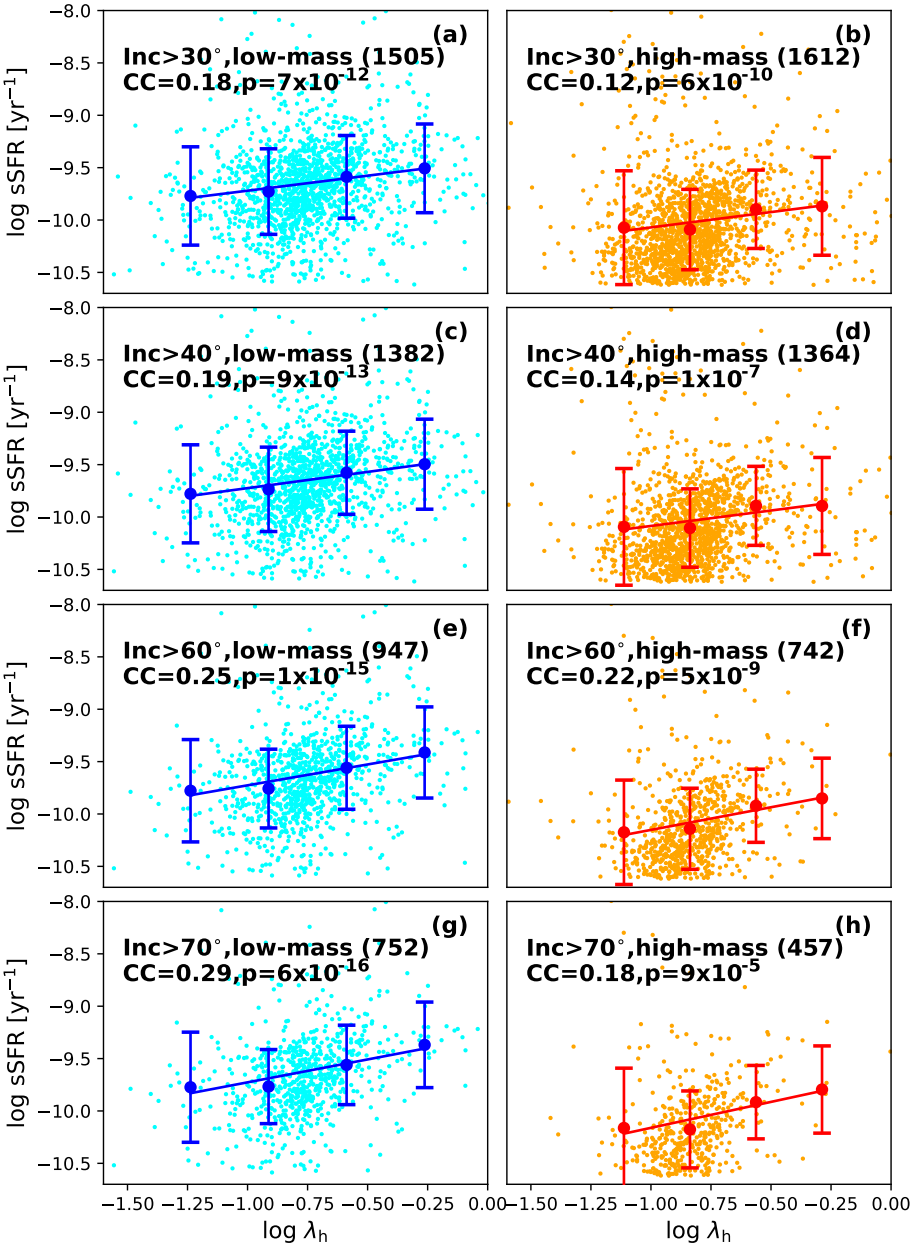

Figure 3. The correlations between sSFR and halo spin for low-mass (left) and high-mass (right) galaxies at the different inclination cutting thresholds. From the top panels to the bottom panels, we show the results for the isolated star-forming galaxies with the inclination cutting thresholds of 30°, 40°, 60°, 70°, respectively. Analogous to Figure 2, the median sSFR values with 1σ error bars for each bin in log λ_h are represented, with the lines indicating the best-fit linear trends. CC and p-value for the subsamples are also shown in the corresponding panels.

from effective radii (R_e) following $R_{\star,d} \simeq R_e/1.678$ (Graham & Driver 2005), where R_e values are taken from our previous work (Rong et al. 2025). While this alternative approach maintains the sSFR–spin correlation (Figure 4), the reduced sample size (due to limited R_e measurements for many ALFALFA galaxies) results in larger p-value and weaker statistical significance.

Third, given the established correlation between surface brightness/density and halo spin (e.g., Cortese et al. 2022; Rong et al. 2025), we must consider whether the observed sSFR–spin correlation could be artificially induced by sample incompleteness at the high-spin end—where galaxies with low surface brightness/density may be underrepresented (Rong et al. 2025). To test this possibility, we split the star-forming galaxy sample into two equal-size subsamples based on stellar SD using measurements from Rong et al. (2025), and examine the sSFR–spin relationship independently for both low-SD and high-SD subsamples. As illustrated in Figure 5, both

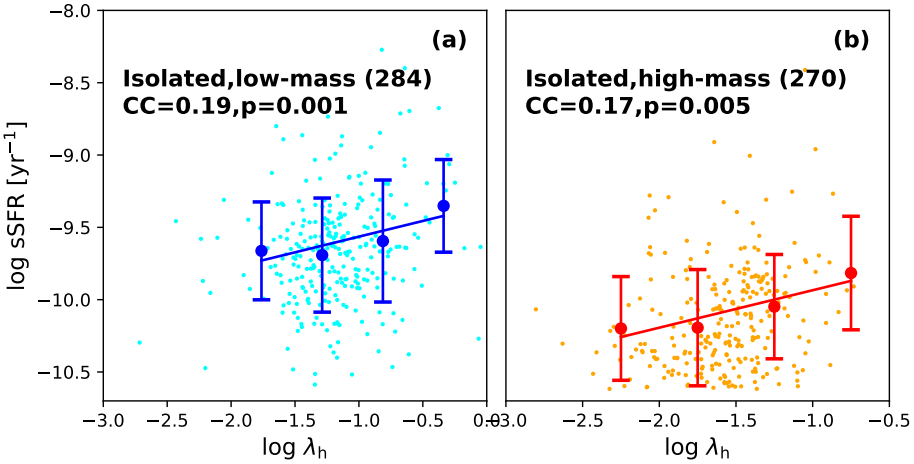

Figure 4. sSFR versus halo spin parameter calculated with the scale length of stellar disk, for isolated low-mass (a) and high-mass (b) star-forming galaxies.

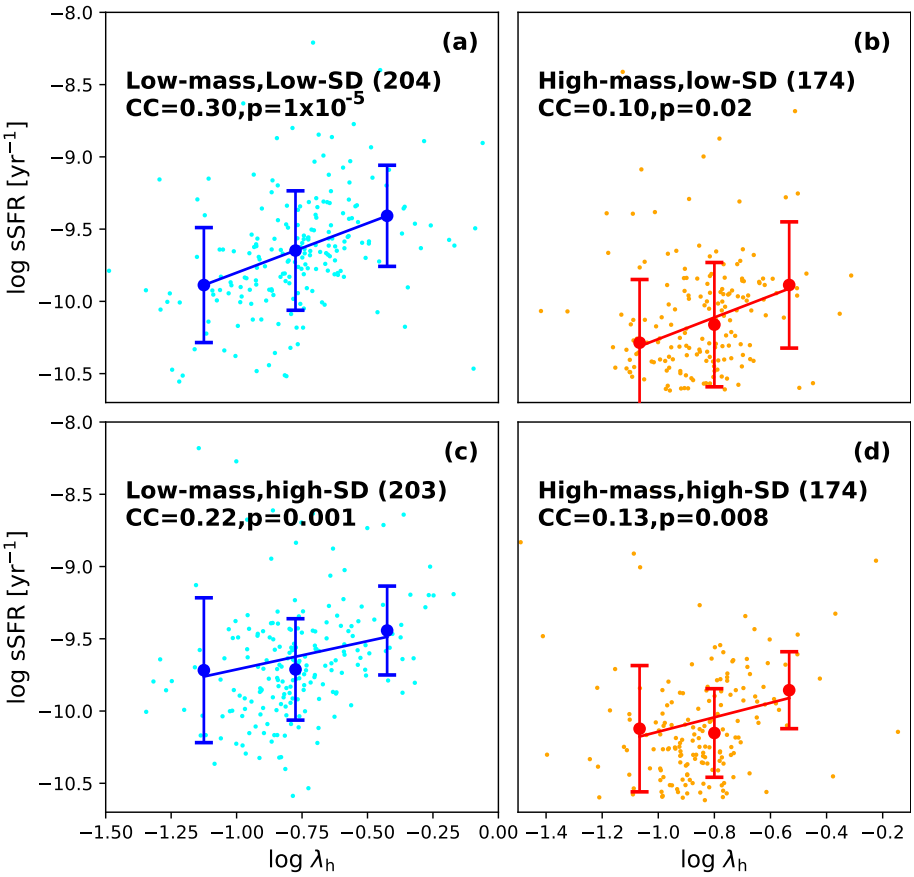

Figure 5. sSFR versus halo spin parameter for low-mass (left) and high-mass (right) star-forming galaxies. The upper and lower panels show the correlation for the low and high surface density subsamples, respectively.

subsamples retain a significant correlation between sSFR and λ_h, demonstrating that the observed trend is intrinsic rather than an artifact of observational biases.

Finally, building upon the established correlation between H I-to-stellar mass ratio and halo spin (Liu et al. 2025), further test the intrinsic nature of the sSFR–spin relationship by dividing our isolated star-forming sample into H I-rich and H I-poor subsamples of equal size. Crucially, both subsamples maintain a statistically significant correlation between sSFR and λ_h (Figure 6). This robust confirmation suggests that the

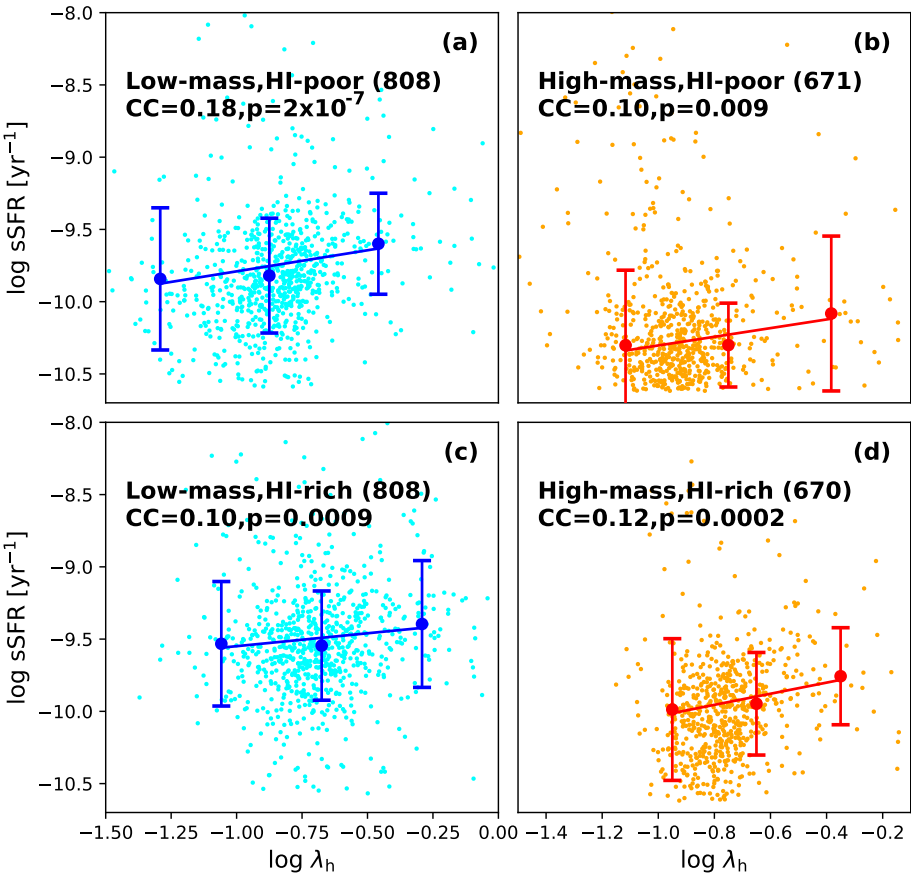

Figure 6. Analogous to Figure 5, this plot shows the sSFR versus halo spin parameter for low-mass (left) and high-mass (right) star-forming galaxies. The upper and lower panels show the correlation for the H I-poor and H I-rich subsamples, respectively.

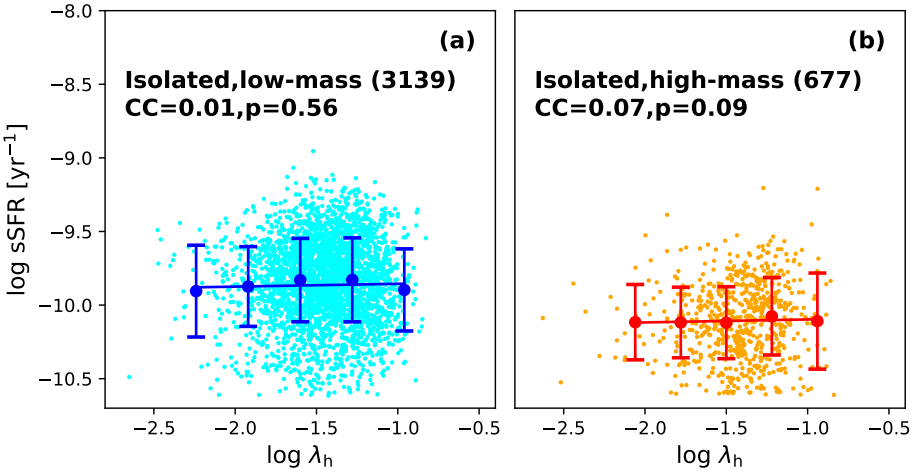

Figure 7. sSFR versus halo spin parameter for low-mass (left) and high-mass (right) isolated star-forming galaxies in TNG50 simulations.

sSFR–spin connection reflects fundamental galactic physics rather than secondary dependencies on H I mass fraction.

Our results show excellent agreement with previous findings from MaNGA IFU data (Cortese et al. 2022), confirming the existence of an sSFR–spin correlation in observational data. However, this relationship is notably absent in the Illustris-TNG50 cosmological simulation (Nelson 2019), where we find no significant correlation between sSFR and λ_h, where we find no significant correlation between sSFR and λ_h for isolated star-forming galaxies at $z \sim 0$. Figure 7 shows the sSFRs

(calculated within $2R_e$) versus λ_h (estimated with the same method of Rodriguez-Gomez 2022) for galaxies. The weak correlation strength (CC $\sim$ 0) and high p-values suggest that current simulations may not fully capture the complex baryonic physics governing this relationship, particularly in their treatment of star formation thresholds and feedback mechanisms.

The observed positive correlation between halo spin and sSFR may be understood through several interconnected physical mechanisms. Galaxies residing in high-spin halos naturally develop more extended, dynamically colder gaseous disks (Mo et al. 1998; Teklu et al. 2015). These morphological characteristics plausibly promote two key conditions for enhanced star formation: (1) elevated gas SDs that exceed local star formation thresholds, and (2) prolonged gas reservoirs that sustain star formation over extended timescales (Kennicutt 1998; Krumholz & McKee 2005). Recent studies (Liu et al. 2025; Rong et al. 2025) provide empirical support for this scenario, demonstrating that high-spin halos indeed host more extended disks with greater gas fractions. The stronger spin–sSFR correlation in low-mass galaxies likely reflects their dominant cold-mode accretion (Kereš et al. 2005). In these systems, the star formation efficiency becomes especially sensitive to angular momentum transport and disk stability (Dekel & Birnboim 2006) as their shallower potential wells are less effective at thermalizing incoming gas flows.

While our analysis demonstrates a clear sSFR–spin correlation in typical star-forming galaxies, we note an important exception: isolated ultra-diffuse galaxies (UDGs). Although UDGs are theoretically predicted to possess high halo spins (Rong et al. 2017), they consistently exhibit suppressed SFRs (Rong et al. 2020). This apparent contradiction can be reconciled by considering that UDGs represent a rare population (van Dokkum et al. 2015) with distinct evolutionary pathways, and that our sample selection criteria explicitly excluded low-sSFR systems, including UDGs. It is worth to note that the sSFR–spin correlation appears to be valid only for actively star-forming galaxies.

Acknowledgments

Y.R. acknowledges supports from the NSFC grants 12273037 and 12522302, the CAS Pioneer Hundred Talents Program (Category B), the USTC Research Funds of the Double First-Class Initiative. This work is supported by the China Manned Space Program with grant Nos. CMS-CSST-2025-A06 and CMS-CSST-2025-A08.

References

Alam, M. P. 2015, ApJS, 219, 12
Amorisco, N. C., & Loeb, A. 2016, MNRAS, 459, L51
Benavides, J. A., Sales, L. V., Abadi, M. G., et al. 2023, MNRAS, 522, 1033
Brinchmann, J., Charlot, S., White, S. D. M., et al. 2004, MNRAS, 351, 1151
Cortese, L., Fraser-McKelvie, A., & Woo, J. 2022, MNRAS, 513, 3709
Dahlem, M., Lisenfeld, U., & Rossa, J. 2006, A&A, 457, 121
Dekel, A., & Birnboim, Y. 2006, MNRAS, 368, 2
Desmond, H., Mao, Y.-Y., Wechsler, R. H., Crain, R. A., & Schaye, J. 2017, MNRAS, 471, L11
Di Cintio, A., Brook, C. B., Macciò, A. V., Dutton, A. V., & Cardona-Barrero, S. 2019, MNRAS, 486, 2535
Diemand, J., Madau, P., & Moore, B. 2005, MNRAS, 364, 367
Durbala, A., Finn, R. A., Crone Odekon, M., et al. 2020, AJ, 160, 271
El-Badry, K. 2018, MNRAS, 473, 1930
Gault, L. 2021, AJ, 909, 19
Giovanelli, R., Haynes, M. P., Kent, B., et al. 2005, AJ, 130, 2598
González, R. E., & Padilla, N. D. 2009, MNRAS, 397, 1498
Graham, A. W., & Driver, S. P. 2005, PASA, 22, 118
Grudić, M. Y., Hopkins, P. F., Faucher-Giguère, C.-A., et al. 2018, MNRAS, 475, 3511
Guo, Q. 2011, MNRAS, 413, 101
Haynes, M. P. 2018, ApJ, 861, 49
Hayward, C. C., Kereš, D., Jonsson, P., et al. 2011, ApJ, 743, 159
Hernandez, X., Park, C., Cervantes-Sodi, B., & Choi, Y.-Y. 2007, MNRAS, 375, 163
Hjorth, J., Gall, C., & Michalowski, M. J. 2014, ApJL, 872, L23
Hopkins, P. F., Quataert, E., & Murray, N. 2012, MNRAS, 421, 3488
Hua, Z., Rong, Y., & Hu, H.-J. 2025a, MNRAS, 538, 775
Hua, Z., Rong, Y., & Hu, H.-J. 2025b, RAA, 25, 041001
Huchra, J. P. 2012, ApJS, 199, 26
Jiang, F. 2019, MNRAS, 488, 4801
Jing, Y.-J., Rong, Y., Wang, J., Guo, Q., & Gao, L. 2021, RAA, 21, 218
Kazantzidis, S., Lokas, E., Callegari, S., Mayer, L., & Moustakas, L. 2011, ApJ, 726, 98
Kennicutt, R. C., Jr. 1998, ApJ, 498, 541
Kereš, D., Katz, N., Weinberg, D. H., & Davé, R. 2005, MNRAS, 363, 2
Kim, J.-h., & Lee, J. 2013, MNRAS, 432, 1701
Kimm, T. 2009, MNRAS, 394, 1131
Kravtsov, A. V., & Vikhlinin, A. A. 2018, AstL, 44, 8
Krumholz, M. R., & McKee, C. F. 2005, ApJ, 630, 250
Liu, S., Rong, Y., Hua, Z., & Hu, H. 2025, RAA, 25, 081001
Mastropietro, C., Moore, B., Mayer, L., et al. 2005, MNRAS, 364, 607
Mayer, L., Governato, F., Colpi, M., et al. 2001, ApJL, 547, L123
Mo, H. J., Mao, S. D., & White, S. D. M. 1998, MNRAS, 295, 319
Moore, B., Katz, N., & Lake, G. 1996, Natur, 379, 613
Nelson, D. 2019, ComAC, 6, 2
Noeske, K. G., Weiner, B. J., & Faber, S. M. 2007, ApJL, 660, 43
Rodriguez-Gomez, V. 2022, MNRAS, 512, 5978
Rong, Y., Guo, Q., Gao, L., et al. 2017, MNRAS, 470, 4231
Rong, Y., He, M., Hu, H., Zhang, H.-X., & Wang, H.-Y. 2024a, arXiv:2409.00944
Rong, Y., Hu, H., He, M., et al. 2024b, arXiv:2404.00555
Rong, Y., Hua, Z., & Hu, H. 2025, RAA, 25, 011001
Rong, Y., Zhu, K., Johnston, E. J., et al. 2020, ApJL, 899, L12
Sales, L. V., Wetzel, A., & Fattahi, A. 2022, NatAs, 6, 897
Saulder, C., van Kampen, E., Chilingarian, I. V., Mikske, S., & Zeilinger, W. W. 2016, A&A, 596, A14
Sawala, T., Frenk, C. S., Fattahi, A., et al. 2015, MNRAS, 448, 2941
Schreiber, C., Elbaz, D., Pannella, M., et al. 2016, A&A, 589, A35
Smith, R., Sánchez-Janssen, R., Beasley, M. A., et al. 2015, MNRAS, 454, 2502
Springel, V. 2000, MNRAS, 312, 859
Teklu, A. F., Remus, R.-S., Dolag, K., et al. 2015, ApJ, 812, 29
Tinker, J. L., Wetzel, A. R., & Conroy, C. 2017, MNRAS, 472, 2504
van den Bosch, F. C. 1998, ApJ, 507, 601
van Dokkum, P. G., Abraham, R., Merritt, A., et al. 2015, ApJL, 798, 45
Wang, J., Koribalski, B. S., Serra, P., et al. 2016, MNRAS, 460, 2143
Yang, H., Gao, L., Frenk, C. S., et al. 2023, MNRAS, 518, 5253
Zhang, C.-P., Zhu, M., Jiang, P., et al. 2024, SCPMA, 67, 219511